Total eigenphase description of multiparticle quantum systems

John L. Bohn

Department of Physics and The James Franck Institute, The University of Chicago, Chicago, Illinois 60637

This paper presents a formalism for studying semianalytically the *development* of a multiparticle quantum-mechanical system outward from its center of mass, casting its dynamics in terms of hyperspherical coordinates which emphasize collective motions of all constituents. The formalism expresses the system's development through an R matrix which varies with the system's hyperradius R, incorporating a greater amount of the dynamics as R grows. Eigenvalues of the R matrix are further transformed into R-dependent phases whose R variation elucidates interactions between alternative degrees of freedom. An initial application to the $^1S^e$ states of helium reveals details of interactions hitherto concealed within numerical treatments.

PACS number(s): 31.10.+z

I. INTRODUCTION

The dynamics of atoms and molecules hinges on transfers of energy, momentum, and angular momentum among the interacting electrons and nuclei, leading, for instance, to the complete rearrangement of molecules in a chemical reaction. In this instructive case, reactant molecules, each with its own stable structure, come together to form a "reaction complex" which then breaks up into various products. The various reactant and product configurations lie in alternative "channels," characterized by an appropriate set of quantum numbers; the essential dynamics asserts itself in the *transition* from the short-range complex to the long-range fragmentation channels. Progress along this transition can be parametrized by a hyperradial coordinate $R = \sqrt{\sum_i m_i r_i^2/M}$ (where $M = \sum_i m_i$, the total mass) describing the overall size of the complex. This paper presents a semianalytic *ab initio* procedure detailing the hyperradial development of an atomic system and demonstrating that the most relevant channel couplings occur in well-defined regions of R marked by degeneracies of channel phases.

Progress of channel development along a radial or hyperradial coordinate is generally studied by reducing the relevant second-order wave equations into pairs of first-order equations better suited to a description of the development as an R-dependent flow [1]. One such transformation reduces wave functions to their R-dependent amplitudes and phase *shifts* relative to a standard set of basis functions [2]. The phase shifts arise in the multichannel context as eigenchannels of an R-dependent "short-range reaction matrix" K; this approach has proven fruitful in two of the simplest nonseparable problems of atomic physics, hydrogen Rydberg diamagnetism [3] and the doubly excited states of helium [4]. Related treatments study the evolution of flux between basis channels, applying the concept to molecular collisions and photoprocesses [5]. An alternative reduction casts one-dimensional wave functions in terms of their amplitude and *total* phase [6–8]. A recent proposal [9] extends this

analysis to the multichannel case by considering an R-dependent R-matrix independent of predetermined basis functions.

Here we systematize the approach of Ref. [9], applying its method to helium, thus complementing and extending the results of [4]. Specifically, we focus on autoionizing transitions in helium, where energy initially shared by both electrons ultimately concentrates on a single electron, ejecting it from the atom. These doubly excited and ionized configurations constitute alternative fragmentation channels analogous to the chemical reactant and product channels above.

For this and similar problems, R-matrix methods [10,11] recognize and exploit the distinction between short- and long-range phenomena by distinguishing "core" and "asymptotic" regions of configuration space. The core region encloses all channel interactions including the doubly excited channel (which cannot extend to infinity at energies below the double-ionization threshold). The problem is solved inside the core by matrix diagonalization or by variational methods, to produce logarithmic derivative boundary conditions at the core's surface. The asymptotic region contains only the ejected electron whose wave functions in the Coulomb plus dipole field of the (distant) He$^+$ ion are known analytically. Standard procedures of the quantum defect theory [12,13] interconnect solutions at the core's boundary, yielding accurate results for scattering phase shifts.

Conventional R-matrix techniques thus reduce the transition region to a single boundary surface, concealing details of interactions within a numerical treatment of the core region, a deficiency we will remove by techniques akin to invariant imbedding [14]. Specifically, we will construct an R matrix explicitly at *each* value R' of the hyperradius, incorporating only the interactions relevant at $R \leq R'$. The R matrix so constructed coincides with the conventional R matrix on the boundary of a core region, yet its elements evaluated throughout the range $R \leq R'$ illustrate the progressive development both of the fragmentation channels and of their mixing. We thus replace previous R-matrix propagation techniques [15,16] that did not concern themselves explicitly with

the development of channel couplings. These techniques divide the radial coordinate into sectors, within which the radial function is approximated by, e.g., Airy functions, leading to approximate Green's functions for propagating the R matrix from one sector boundary to the next. The alternative "diabatic by sector" method diagonalizes the hyperspherical Hamiltonian [Eq. (1), below] at a representative fixed R within each sector, then connects the sector solutions to form a final R matrix [17], demonstrating the utility of hyperspherical coordinates in an accurate computational scheme, but without displaying the details of channel development. We replace these techniques with a more direct first-order differential equation for the R matrix, whose eigenchannels reveal the development of the electron pair's dynamics.

The R-matrix eigenchannels developed here bear some relation to the well known adiabatic channels that approach the problem by treating R as a "slow" coordinate in the sense of the Born-Oppenheimer approximation [18,19]. The adiabatic approximation results in a set of potential curves in R, whose bound states approximate the resonant levels of doubly excited helium but must be coupled in a separate step to describe autoionizing transitions. The R-matrix eigenchannels, by contrast, embrace both the adiabatic channels and their coupling. Thus while adiabatic channels can describe autoionizing levels, the R-matrix eigenchannels display their autoionizing widths as well, as we demonstrate here for several low-lying autoionizing states of helium. Inclusion of the full coupling becomes especially relevant at higher excitation energies, where numerous adiabatic channels overlap, impairing their ability to describe resonances [20]. The R-matrix eigenchannels should thus provide a useful fully wave mechanical description of the approach to the threshold for double ionization in helium, to be pursued in future work.

II. CHANNEL DEVELOPMENT FORMALISM

This section derives the equations for the flow of the R matrix of a general $\mathcal{N}$-body atomic or molecular system outward from its center of mass, focusing on the first-order equations governing the eigenchannel functions and their phases. We will specialize to the helium atom in Sec. III.

A. Formulation in hyperspherical coordinates

The hyperspherical coordinates for an $\mathcal{N}$-body system, referred to its center of mass, consist of the hyperradius R and of $(3\mathcal{N} - 4)$ angles—signifying, for instance, the directions and relative lengths of a set of Jacobi coordinates [21]—denoted collectively as Ω. In these coordinates the Hamiltonian resembles that of a single particle in a Coulomb potential [22,23],

$$H = -\frac{1}{2M}\left[\frac{\partial^2}{\partial R^2} - \frac{\Lambda^2 + (3\mathcal{N} - 4)(3\mathcal{N} - 6)/4}{R^2}\right] - \frac{C(\Omega)}{R},$$

$$(1)$$

whose operators Λ^2 and $C(\Omega)$ represent a generalized squared angular momentum and effective charge products, respectively. Centrifugal forces dominate the motion at small R, Coulomb forces at large R, just as for a single particle; the noncommutativity of Λ^2 and $C(\Omega)$ drives the dynamical transition between these regimes.

The similarity of the Hamiltonian (1) to a single-particle Hamiltonian suggests separating its dynamics into nearly independent channels, each mimicking the motion of a single particle in an effective radial potential, which interact only weakly to complete the description of the system's dynamics. Adiabatic treatments have proceeded in this direction, disregarding the R derivatives in (1) and diagonalizing the centrifugal plus Coulomb interactions to produce effective potentials [18,19]. Such weakly interacting channels are reminiscent of "quasiparticle" excitations in many-body theory [24]. Indeed, many-body treatments of atoms employ quasiparticle notions, generally in the form of Hartree-Fock wave functions [25]. In this section we describe the evolution of eigenchannels of total phase which reflect electron correlations more fully than either the adiabatic or Hartree-Fock approximations.

Small-R eigenchannels amount to eigenchannels of Λ^2, represented by hyperspherical harmonics $Y_\beta(\Omega)$ [21], which progressively mix as R grows. Here, Y_β represents an eigenfunction of Λ^2 with eigenvalue $\lambda(\lambda + 3\mathcal{N} - 5)$ for an $\mathcal{N}$-body system. The index β denotes a set of quantum numbers, consisting of λ and additional labels that distinguish harmonics degenerate in λ. The set β is not unique, depending on the choice of coordinates Ω; we therefore do not specify β in this section.

A full energy eigenstate ψ of (1) superposes different harmonics Y_β with R-dependent coefficients,

$$\psi_{\beta_0}(\Omega, R) = \sum_\beta Y_\beta(\Omega) F_{\beta\beta_0}(R),$$

$$(2)$$

where the additional index β_0 identifies the short-range channel in which ψ originates through the boundary conditions on F:

$$F_{\beta\beta_0} \propto R^{\lambda + (3\mathcal{N} - 4)/2}\delta_{\beta\beta_0} \quad \text{as} \quad R \to 0.$$

$$(3)$$

[Fock [26] has demonstrated that a series expansion of the helium wave function near $R = 0$ must involve terms logarithmic in R. Equation (3) ignores these terms, yet proves adequate for our present semiquantitative purposes.] Inserting (2) into the Schrödinger equation with Hamiltonian (1) and projecting onto $Y_{\beta'}$ yields close-coupling-type equations for F:

$$\frac{d^2 F_{\beta\beta_0}}{dR^2} = -\sum_{\beta'} k_{\beta\beta'}^2 F_{\beta'\beta_0},$$

$$(4)$$

whose channel coupling originates in the squared wave number matrix

$$k_{\beta\beta'}^2(R) = \int d\Omega\, Y_\beta(\Omega) \left[2ME - \frac{\Lambda^2 + (3\mathcal{N} - 4)(3\mathcal{N} - 6)/4}{R^2} + 2M\frac{C(\Omega)}{R} \right] Y_{\beta'}^*(\Omega)$$

$$= \left[2ME - \frac{[\lambda + (3\mathcal{N} - 5)/2]^2 - 1/4}{R^2} \right] \delta_{\beta\beta'} + 2M\frac{C_{\beta\beta'}}{R}. \tag{5}$$

B. Formulation through radial eigenphases

R-matrix theory solves (4) within a core region, casting the net effect of channel coupling as an R matrix on the core's boundary. The R-matrix $\mathcal{R}_{\beta\beta'}$ (denoted by $\mathcal{R}$ to distinguish it from the hyperradius) relates F to its normal derivative,

$$\sum_{\beta'} \mathcal{R}_{\beta\beta'} \frac{dF_{\beta'\beta_0}}{dR} - F_{\beta\beta_0} = 0, \tag{6}$$

providing a multichannel analog of the logarithmic derivative that serves as a boundary condition for each channel's asymptotic wave function. Here we view the core as an ever-enlarging hypersphere that accommodates increasing amounts of the interaction as R grows [2]. The R-matrix $\mathcal{R}$ thus relates F to dF/dR according to (6) at *each* R, satisfying the differential equation generated by differentiating (6), inserting (4), and multiplying on the right by $(dF/dR)^{-1}$:

$$\frac{d\mathcal{R}_{\beta\beta'}}{dR} = \delta_{\beta\beta'} + \sum_{\gamma\gamma'} \mathcal{R}_{\beta\gamma} k_{\gamma\gamma'}^2 \mathcal{R}_{\gamma'\beta'}. \tag{7}$$

Initial conditions for $\mathcal{R}$ follow from those for F [Eq. (3)],

$$\mathcal{R}_{\beta\beta'} \to \frac{R}{\lambda + (3\mathcal{N} - 4)/2} \delta_{\beta\beta'} \quad \text{as} \quad R \to 0. \tag{8}$$

These nonsingular boundary conditions motivate working with $\mathcal{R}$ rather than with its inverse, the logarithmic derivative matrix.

Equation (7) displays the propagation of $\mathcal{R}$ under the influence of the "dressed" interaction $\mathcal{R}k^2\mathcal{R}$, whose significance becomes apparent by expressing (7) in a basis of eigenchannels $|\rho\rangle$ of $\mathcal{R}$,

$$\mathcal{R}_{\beta\beta'} = \sum_\rho \langle\beta|\rho\rangle \tan\phi_\rho \langle\rho|\beta'\rangle. \tag{9}$$

Equation (9) casts the eigenvalues of $\mathcal{R}$ as tangents of eigenphases ϕ_ρ by analogy with casting those of a reaction matrix K as tangents of phase shifts [13,3]. This identification of phases follows the practice in Ref. [27] of assigning to any single-channel radial function $f(R)$ a phase $\phi(R)$ based on its "R matrix,"

$$\tan\phi = \frac{f}{df/dR}. \tag{10}$$

[Strictly speaking, the right-hand side of (10) should contain a dimensional factor with units of reciprocal length; we set this factor to 1 a.u. in the following without

harming our general conclusions.] The channel phases thus identify radial nodes in each channel as they pass through multiples of π.

The radial derivative of (9), projected onto the eigenchannels, yields

$$\sum_{\beta\beta'} \langle\rho|\beta\rangle \frac{d\mathcal{R}_{\beta\beta'}}{dR} \langle\beta'|\rho'\rangle = \frac{d\tan\phi_\rho}{dR} \delta_{\rho\rho'}$$
$$+ \sum_\beta \frac{d\langle\rho|\beta\rangle}{dR} \langle\beta|\rho'\rangle$$
$$\times (\tan\phi_\rho - \tan\phi_{\rho'}), \tag{11}$$

whose first term on the right-hand side expresses the variation of the eigenvalues of $\mathcal{R}$, whereas its second term accounts for the accompanying variation of the eigenchannels. (An analogous equation for the eigenchannels of a matrix appears, e.g., in [3].) Similarly, a joint projection of (7) onto $\langle\rho|$ and $|\rho'\rangle$ yields

$$\sum_{\beta\beta'} \langle\rho|\beta\rangle \frac{d\mathcal{R}_{\beta\beta'}}{dR} \langle\beta'|\rho'\rangle = \delta_{\rho\rho'} + \tan\phi_\rho \bar{k}_{\rho\rho'}^2 \tan\phi_{\rho'}, \tag{12}$$

by introducing the notation

$$\bar{k}_{\rho\rho'}^2 = \sum_{\beta\beta'} \langle\rho|\beta\rangle k_{\beta\beta'}^2 \langle\beta'|\rho'\rangle \tag{13}$$

to denote the effective coupling in the ρ, ρ' basis. Comparison of diagonal elements of the right-hand sides of (11) and (12) produces the differential equation for the eigenphase ϕ_ρ:

$$\frac{d\phi_\rho}{dR} = \cos^2\phi_\rho + \bar{k}_{\rho\rho}^2 \sin^2\phi_\rho. \tag{14a}$$

Comparison of off-diagonal terms yields, after further projection onto a basis element $|\beta\rangle$,

$$\frac{d\langle\rho|\beta\rangle}{dR} = \sum_{\rho'\neq\rho} \frac{\sin\phi_\rho \bar{k}_{\rho\rho'}^2 \sin\phi_{\rho'}}{\sin(\phi_\rho - \phi_{\rho'})} \langle\rho'|\beta\rangle. \tag{14b}$$

The eigenchannel $|\rho\rangle$ corresponds to the "free" quasiparticle in many-body theory [24], by interacting with itself through the dressed effective interaction in (14a) as it propagates. The effective interaction, in turn, represents the collective effect of various $|\beta\rangle$ channels relevant to constructing and maintaining $|\rho\rangle$.

The channels themselves develop via the dressed interactions in (14b), coupled by off-diagonal elements of $\bar{k}^2$. The total energy E does not appear explicitly in (14b) since its portion of $\bar{k}^2$ is diagonal in ρ, but E does

influence the channels implicitly through (14a). The ρ channels are thus "dynamically selected," adapting themselves to the circumstances prevailing in different energy ranges, thus superseding the adiabatic channels defined independently of energy and of hyperradial-hyperangular correlations. In addition, these channels can follow the system into its various fragmentations, since the global structure of the hypersphere becomes irrelevant when a channel localizes in a narrow hyperangular neighborhood of a fragmentation direction Ω_0. R then plays the role of a distance between two fragments whose essentially one-dimensional motion is described by the corresponding eigenphase.

Equations (14) raise numerical difficulties when two phases become nearly degenerate (modulo π) causing the denominator in (14b) to vanish. In the results reported here our policy has been to integrate the R-matrix equations (7) directly, away from poles of $\mathcal{R}$; only near the poles do we switch to its eigenphase representation (14).

III. BOUND AND RESONANT ^1S LEVELS OF HELIUM

A. Hyperspherical harmonics for two-electron atoms and ions

We specify here angular coordinates Ω and quantum numbers β for the helium atom, setting $\mathcal{N} = 3$ and restricting our attention to ^1S symmetry, which serves to illustrate general features. We fix the nucleus at the center of mass of the atom, thus disregarding mass polarization effects of order $\sim m_{\mathrm{electron}}/m_{\mathrm{proton}}$. We then take as hyperangles the direction angles (θ_1, φ_1), (θ_2, φ_2) of the two electrons as well as the radial correlation angle α defined by $\alpha = \tan^{-1}(r_2/r_1)$. The quantum numbers β consist of the orbital angular momenta l_1 and l_2 of the two electrons and of a radial correlation quantum number n_α enumerating the nodes in α. These quantum numbers combine into the "grand angular momentum" quantum number $\lambda = l_1 + l_2 + 2n_\alpha$. In addition, the individual angular momenta are coupled into the total angular momentum L and its z projection M, omitted from the notation in the following. The hyperspherical harmonics $Y_{l_1 l_2 n_\alpha}$, which diagonalize Λ^2,

$$\Lambda^2 Y_{l_1 l_2 n_\alpha} = \lambda(\lambda + 4) Y_{l_1 l_2 n_\alpha}, \tag{15}$$

are combinations of standard spherical harmonics in (θ_i, φ_i) and Jacobi polynomials in $\sin 2\alpha$ described elsewhere [21,28].

Each channel $(l_1 l_2 n_\alpha)$ contributes significantly only when it "emerges from its centrifugal barrier," i.e., when its Coulomb forces become comparable to its centrifugal forces. The Coulomb operator $C(\Omega)$ is nearly diagonal when expressed in the $(l_1 l_2 n_\alpha)$ basis, with off-diagonal elements suppressed typically by an order of magnitude relative to diagonal elements [29]. Radial development in the diagonal portion of the combined Coulomb and centrifugal potentials

$$V_{l_1 l_2 n_\alpha}(R) = \frac{(\lambda + 2)^2 - 1/4}{R^2} - \frac{\langle l_1 l_2 n_\alpha | C | l_1 l_2 n_\alpha \rangle}{R} \tag{16}$$

therefore constitutes a zeroth-order approximation. Figure 1 shows several of these potentials for low values of λ. Roughly speaking, each channel emerges from its centrifugal barrier when $V_{l_1 l_2 n_\alpha}$ first drops to zero (although the channel accumulates some phase at smaller R). This emergence occurs for each λ at smaller radii for larger C, the largest of which corresponds to the largest value of n_α [30], because these harmonics incorporate the most "asymmetric stretch" motion, allowing each electron to dwell longer near the nucleus and lowering the effective potential. The various values of C for each λ cause the channels to emerge from their barriers roughly in groups, indexed by the sum $\gamma = l_1 + l_2 + n_\alpha$, rather than by λ, as indicated in Fig. 1. In the following we enumerate basis harmonics in order of ascending γ, unless stated otherwise. For example, the set of basis channels pictured in Fig. 1 is identified by $\gamma = 0, 2, 4$.

B. Bound states of helium

Bound states occur for those energies at which a channel phase rises suddenly at large R through a multiple of π. Figure 2 illustrates the general phase behavior with a six channel example at an energy 0.05 a.u. above the helium ground state, -2.903 a.u. Only one channel, labeled $\rho = 1$ in the figure, accumulates significant phase; we term it the ground channel. The remaining channels are far from accumulating enough phase to begin supporting bound states. The next two channels have nevertheless separated themselves from the rest, representing the beginnings of the two channels containing the two series of resonances converging to the $N = 2$ ionization threshold of helium. The remaining channels likewise represent seeds of doubly excited channels that play a role at still higher energies.

The ground channel's behavior displays features common to all closed channel phases. The profile of ϕ_1 can be divided into two regions of R with different behavior:
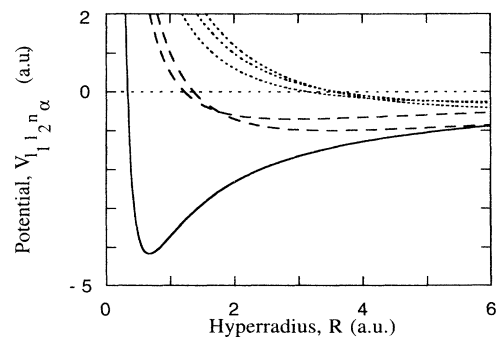

FIG. 1. Diagonal portions of the centrifugal plus Coulomb potential $V_{l_1 l_2 n_\alpha}$ [Eq. (16)] for small values of $\gamma = l_1 + l_2 + n_\alpha$. Solid line: $\gamma = 0$; dashed lines: $\gamma = 2$; dotted lines: $\gamma = 4$. Potentials sharing a common value of γ cross zero energy at approximately the same value of R.

(1) At short ranges, where the channel kinetic energy $\frac{1}{2}\bar{k}_{11}^2$ remains positive, the phase ϕ_1 accumulates at a nearly uniform rate, modulated by the oscillating $\cos\phi_1$ and $\sin\phi_1$ terms in (14a) [these oscillations become more pronounced in higher lying states that accumulate phase more rapidly.]; and (2) further out (at $R \sim 1.8$ a.u. in Fig. 2), the channel kinetic energy becomes negative, causing the channel wave function to switch from freely propagating to tunneling behavior. Here ϕ_1 ceases rising at its previous rate, beginning instead to level off, as does the more familiar Milne phase [8]. The phase thus exhibits the important property that its gradient, which represents a velocity, vanishes rapidly in the tunneling region.

The profile of ϕ_1 far into the tunneling region depends sensitively on the total energy E. If E coincides exactly with the energy of a bound state, then the channel wave function has the convergent form $f_\rho \sim \exp(-\kappa_\rho R)$, with

$$\kappa_\rho = \sqrt{-\bar{k}_{\rho\rho}^2(R \to \infty)}. \qquad (17)$$

This behavior leads to the limiting phase $\phi_\rho \sim \tan^{-1}(-1/\kappa_\rho) + n\pi$ as $R \to \infty$, where n denotes the number of ϕ_ρ passages through π. The dashed lines in Fig. 2 indicate these limiting values for the energies displayed, referred to the first ionization threshold of helium; ϕ_1 indeed tends at first toward this limit. If,

however, E fails to coincide with a bound state energy E_{BS}, the divergent wave function $f_\rho \sim \exp(\kappa_\rho R)$ leads to the phase $\phi_\rho \sim \tan^{-1}(1/\kappa_\rho) + n\pi$ if $E < E_{\mathrm{BS}}$, or $\tan^{-1}(1/\kappa_\rho) + (n+1)\pi$ if $E > E_{\mathrm{BS}}$, as happens in Fig. 2. The sudden change in the course of ϕ_1 (at $R \sim 4.5$ a.u. in Fig. 2) occurs when the channel wave function begins to diverge; this change therefore moves to larger R as E approaches E_{BS} more closely. The profiles in Figs. 2(a) and 2(b) represent unphysical situations with divergent wave functions; the phase would behave more smoothly if the total energy were tuned exactly. The exaggerated large-R behavior of ϕ_1 thus does not correspond to any observable feature, yet proves useful in identifying a bound state's level.

The ground channel phase ϕ_1 attains the value π at an energy between those pictured in Figs. 2(a) and 2(b), identifying an approximate ground state energy of -2.849 a.u. This result, 0.054 a.u. *higher* than the experimental value, can be understood as follows: while the short-range dynamics determines most of the phase, long-range behavior of the effective channel potential in (14a) determines sensitively the long-range details of the phase. This channel potential represents the Coulomb interaction $C(\Omega)$ averaged over the channel eigenfunction

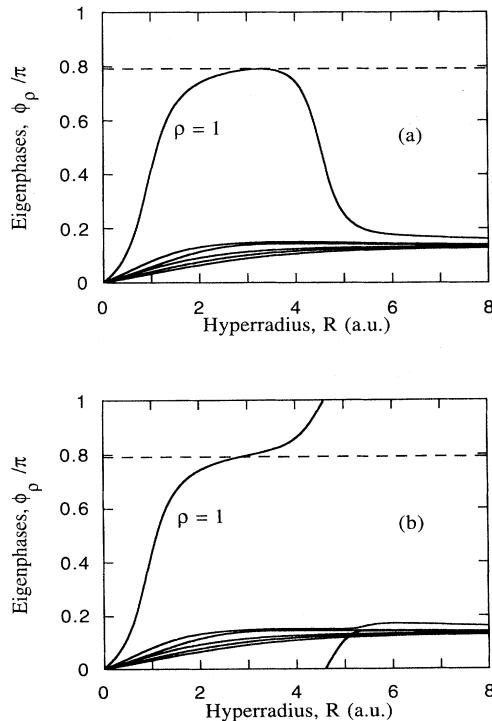$$\Psi_\rho \equiv \sum_\beta \langle \rho|\beta\rangle Y_\beta(\Omega) \qquad (18)$$

at each R; it depends accordingly on the adequacy of the set of harmonics $\{Y_\beta\}$ to describe fine details of Ψ_ρ. Ψ_1 seeks to localize in regions of Ω of lowest potential (therefore of highest phase). A limited set of harmonics thus raises the effective long-range Coulomb potential, resulting in a high estimate of the ground state energy. Our estimate of E_0 should decrease monotonically with increasing size of the basis set of harmonics; Table I verifies this surmise. The converged result, with 21 harmonics, $E_0 = -2.897$, compares well with experiment.

A smaller number of harmonics actually suffices to attain this convergence. The electrons become asymmetrically distributed ($r_1 \gg r_2$ or $r_2 \gg r_1$) for $R > 2$ a.u. since the energy proves insufficient to transport both electrons to large radii. The angular function thus localizes in the potential "valleys" ($\alpha \sim 0, \pi/2$), requiring harmonics with large values of n_α for its description. We therefore choose a basis set of harmonics consisting of the "lowest" six, i.e., those with $\gamma = 0, 2, 4$, plus the high-n_α harmonics $(0,0,6)$, $(0,0,8)$, $(0,0,10)$, and $(0,0,12)$. This choice achieves the same accuracy with only ten ba-

FIG. 2. Eigenphases (modulo π) ϕ_ρ/π, calculated in a six-channel approximation, at the pair of total energies (a) $E = -2.850$ a.u. and (b) $E = -2.849$ a.u. The bound-state energy, E_{BS}, lies between these values, as evidenced by the passage of ϕ_1 through π in (b), but not in (a). The dashed line indicates the limiting value of ϕ_1 if the calculation had been performed at the exact binding energy $E \equiv E_{\mathrm{BS}}$.

TABLE I. Convergence of the ground-state energy with an increasing number of harmonic channels.

$\gamma_{\max}$	Number of channels	Ground-state energy (a.u.)
0	1	-2.500
2	3	-2.782
4	6	-2.849
6	10	-2.880
8	15	-2.891
10	21	-2.897

sis channels; greater accuracy awaits our optimization of the numerical procedure.

The close agreement between E_0 and the experimental ground state suggests that the ground channel alone comprises the bulk of the ground state correlations. Figure 3 compares three ground channel eigenfunction components to those of the lowest-energy adiabatic function. The two sets of functions differ primarily in the range $R \sim 3\text{-}4$ a.u., which coincides with the region of greatest coupling between the lowest adiabatic channel and the next higher adiabatic channel; the R-matrix eigenchannel already incorporates the effects of this coupling. The adiabatic channel, governed by potential energy at fixed R, proceeds as quickly as possible into the potential valleys, thus acquiring higher harmonics rapidly with R. The R-matrix eigenchannel, by contrast, retains a greater $\lambda = 0$ component, allowing Ψ_1 to hold higher amplitude on the potential "ridge" ($\alpha \sim \pi/4$), where the electrons achieve comparable excitation. Figure 4 illustrates this contrast by showing the adiabatic and ground channel functions at $R = 3.0$ a.u., with $\hat{\mathbf{r}}_1 = -\hat{\mathbf{r}}_2$. At larger R, Figure 3 shows that the two types of channels tend to agree, since correlations become less important and both channels describe valley localization.

Passage of ϕ_1 through additional multiples of π at higher energies generates the entire Rydberg series of $1sns$ bound states. A full calculation of the behavior of ϕ_1 proves unnecessary, however, since the electrons remain essentially independent beyond a core radius R_0. We therefore follow conventional R-matrix theory, identifying two relevant regions of R: $R < R_0$, where ϕ_1 varies only slowly with energy and represents all strong correlations, and $R > R_0$, where the wave function describes a single outer electron in the Coulomb field of the $\mathrm{He^+}$ ion. In the outer region, we employ the approximation $R \sim r_{\mathrm{outer}}$ and propagate ϕ_1 as an independent channel phase subject to a Coulomb potential with unit charge. ϕ_1 can thus be computed on a coarse energy mesh in the inner region and on a fine energy mesh in the outer region. Table II presents results for the $1sns$ series calcu-
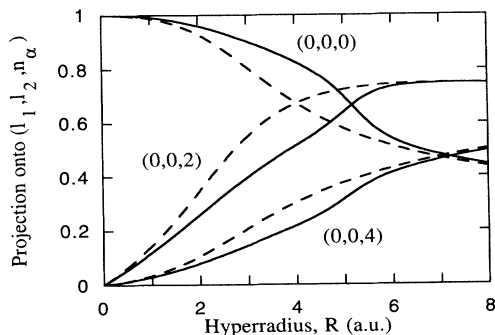
FIG. 3. Solid curves: R dependence of the three dominant components $\langle \rho | l_1 l_2 n_\alpha \rangle = \langle 1|000\rangle$, $\langle 1|002\rangle$, and $\langle 1|004\rangle$ of the ground channel, evaluated at $E = -2.850$ a.u. Dashed curves: the corresponding components of the lowest adiabatic channel. The R matrix and adiabatic channels closely agree at small and at large R, differing primarily in the range $R \sim 3\text{-}4$ a.u.
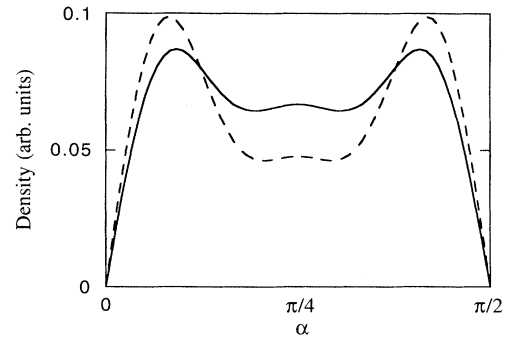
FIG. 4. Solid curve: dependence of the R-matrix channel function Ψ_1 [Eq. (18)] on the hyperangle $\alpha = \tan^{-1}(r_2/r_1)$, holding $\cos\theta_{12} = \hat{\mathbf{r}}_1 \cdot \hat{\mathbf{r}}_2 = -1$ constant, at the hyperradius $R = 3.0$ a.u. Dashed curve: the corresponding dependence of the adiabatic channel function. The R-matrix channel incorporates the full interaction, enabling it to hold a greater amplitude on the potential ridge ($\alpha = \pi/4$).

lated with a core radius of $R_0 = 5.0$ a.u. As n increases, the channel extends to larger R where the approximation $R \sim r_{\mathrm{outer}}$ improves, improving also the estimates of the energies.

C. Autoionizing states below $N = 2$

Below the threshold for ionization to the $N = 2$ levels of the $\mathrm{He^+}$ ion, the $\mathrm{He}(^1S)$ atom possesses two Rydberg series of autoionizing resonances, denoted in the adiabatic scheme as $_N(K,T)_n^A = {}_2(+1,0)_n^+$ and $_2(-1,0)_n^+$ [19]. These two series correspond roughly to "$2sns$" and "$2pnp$" series, although electron-electron angular correlations invalidate these independent electron quantum numbers.

Figure 5 illustrates the behavior of the channel phases ϕ_ρ at a pair of energies near the $_2(+1,0)_2^+$ resonance, calculated with an 18-element basis incorporating $\gamma = 0$, 2, 4, 6, and 8, along with $(0,0,n_\alpha)$ for $n_\alpha \le 14$ and $(1,1,n_\alpha)$ for $n_\alpha \le 12$ (the figure shows only the ten highest phases, for clarity). The ground channel $\rho = 1$ is open at these energies, representing the $1s\epsilon s$ continuum states of helium; its phase ϕ_1 accordingly climbs through many multiples of π, enumerating its radial nodes. This cycling of ϕ_1 produces an array of avoided crossings of ϕ_1 with the other eigenphases, providing loci for the interaction of the continuum channel with the bound channels. Two

TABLE II. Total energies E, in atomic units, of several singly excited states of helium. The third column shows for comparison the experimental values in Ref. [31].

Level	Present result (a.u.)	Experiment (a.u.)
$1s2s$	-2.1196	-2.1463
$1s3s$	-2.0554	-2.0616
$1s4s$	-2.0311	-2.0339
$1s5s$	-2.0199	-2.0215

distinct regions of R manifest themselves in Fig. 5: a core region, $R < 7$ a.u., which is insensitive to variations in the total energy, and an asymptotic region, $R > 7$ a.u., which is altered significantly by the passage of the total energy through a resonance. The core region contains all relevant channel interactions, as in a typical R-matrix calculation, while the asymptotic region exhibits the fine details of phase correlations that usually emerge only upon application of boundary conditions at $R \to \infty$.

Deep into the asymptotic region the R matrix becomes nearly diagonal, since its channels diagonalize the (dominant) Coulomb interaction. All closed channel phases tend then to their standard limits $\phi_\rho \to \tan^{-1}(1/\kappa_\rho) + n\pi$ at $R \to \infty$. This decoupling of channels affords trivial elimination of closed channels [12,13], channel by channel. The open channel phase must therefore already represent the effects of boundary conditions at $R \to \infty$, manifested in Fig. 5 as large avoided crossings for $R > 7$ a.u. Figure 6 verifies this effect, showing the variation of the channel phases with energy at $R = 15.0$ a.u. Only ϕ_1 varies significantly at this energy, rising by $\sim \pi$ as the energy passes through the resonance. The energy derivative of ϕ_1 yields a resonance profile for the $_2(+1,0)_2^+$ resonance, with position $E = -0.769$ a.u. and width $\Gamma = 0.138$ eV, as compared with the experimental values $E = -0.778$ a.u. and $\Gamma = 0.138 \pm 0.015$ eV [32], and calculated values of $E = -0.777$ a.u. and $\Gamma = 0.120$ eV [17]. Similarly, the passage of ϕ_3 through π signals the
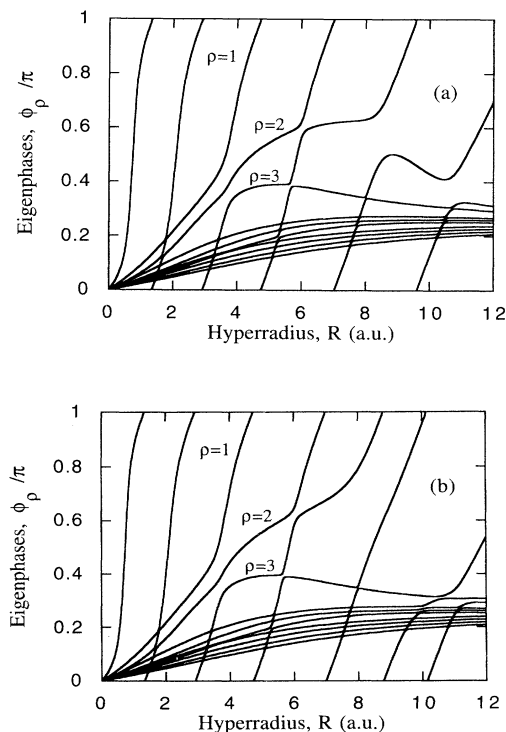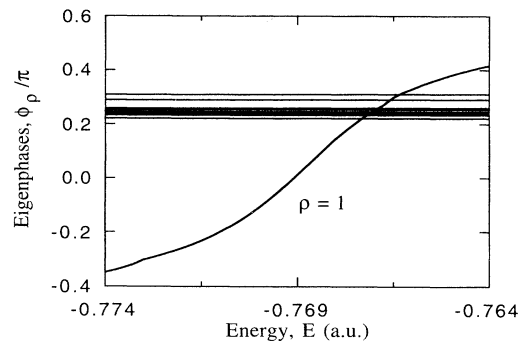

FIG. 6. Energy dependence of the eigenphases ϕ_ρ/π evaluated at $R = 15$ a.u. The ground channel phase ϕ_1 rises by nearly π, identifying the $_2(+1,0)_2^+$ resonance, while the remaining closed channel phases vary little with increasing energy.

$_2(-1,0)_2^+$ resonance, with energy $E = -0.6147$ a.u. and $\Gamma = 3.9 \times 10^{-3}$ eV, compared to the calculated results $E = -0.6218$ a.u. and $\Gamma = 4.9 \times 10^{-3}$ eV [17]. Thus the channel phases identify both bound states and resonances *without* applying long-range boundary conditions explicitly, by accounting for the radial nodal structure.

The total phase description of the $_2(+1,0)_2^+$ resonance presented here complements its phase *shift* description in Ref. [4], whose Fig. 3(a) displays the R-dependent phase shift $\pi\tau$ in the open adiabatic channel. The large avoided crossings of the ϕ_ρ's at $R \sim 3.5$ a.u. correspond to the main accumulations of τ. Notice that ϕ_1 has passed through a full 2π at this hyperradius, so that the $\rho = 1$ and $\rho = 2$ channels couple *in phase*, a conclusion noted in Fig. 4 of Ref. [4]. The in-phase driving of the closed channel by the open channel is the primary means of resonant excitation. Additional phase crossings occur near $R \sim 6.0$ a.u. where the channels meet with a phase difference of π, hindering their coupling. This phase lag between ϕ_1 and ϕ_2 reverses the sign of the interaction [Eq. (14b)], reversing the course of τ in Fig. 3(a) of Ref. [4], a reversal that had previously appeared mysterious. The resulting "anticoupling" would de-excite the resonance, were it not for its relative weakness compared to the coupling at $R \sim 3.5$ a.u. owing to the greater localization of the channels at larger R. The resonance's root lies thus at $R \sim 3.5$ a.u. but its details develop as it progresses further outward.

The behavior of the R-matrix eigenchannel function Ψ_2 [Eq. (18)] in the vicinity of the main crossing reveals the character of the resonance's excitation. Figure 7(a) shows Ψ_2 as a density plot in the hyperangles α and $\theta_{12} = \cos^{-1}(\hat{\mathbf{r}}_1 \cdot \hat{\mathbf{r}}_2)$ at $R = 4.0$ a.u. as the channel emerges from the crossing. Figure 7(b) shows for comparison the corresponding adiabatic channel function at the same radius. Both calculations display dominant localization near the potential ridge ($\alpha = \pi/4, \theta_{12} = \pi$), but the adiabatic channel also contains significant amplitude in the potential valleys ($\alpha \sim 0$ or $\pi/2$). The $\rho = 2$ channel, by contrast, remains more tightly confined away from the valleys. This confinement results from a greater admixture of the harmonic Y_{110} in the $\rho = 2$ channel

FIG. 5. Eigenphases (modulo π) ϕ_ρ/π in an 18-channel calculation at the pair of total energies (a) $E = -0.78$ a.u. and (b) $E = -0.76$ a.u. The $_2(+1,0)_2^+$ resonance lies between these energies, as discussed in the text.
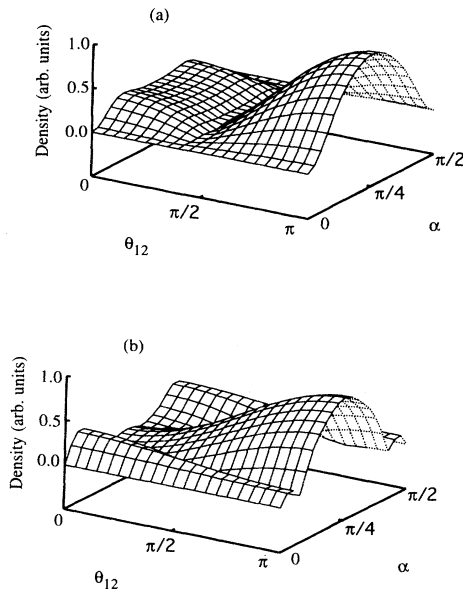
(a)

(b)

FIG. 7. (a) Density plot of the R-matrix channel function Ψ_2 [Eq. (18)] in the (α, θ_{12}) plane for $R = 4.0$ a.u. showing its concentration of amplitude on the potential ridge $(\alpha = \pi/4, \theta_{12} = \pi)$. (b) The corresponding adiabatic $_2(+1,0)^+$ channel function, showing amplitude in the valleys as well as on the ridge. The fully correlated R-matrix channel exhibits greater localization, as in Fig. 4.

than in the adiabatic channel. The present and more accurate channel thus deviates even further from its independent electron description by increasing the "$2p^2$" contribution to the "$2s^2$" state. Excitation of the resonance therefore drives the electron pair *up the ridge*, a mechanism that should prove crucial to the development of the Wannier ridge states at energies approaching the threshold for double ionization (and lying at correspondingly larger values of R) [33]. As R grows beyond 4.0 a.u. $\rho = 2$ "relaxes," growing more like the adiabatic channel in Fig. 7(b).

Direct integration of the R matrix to large R proves

TABLE III. Energies in atomic units of the $_2(+1,0)_n^+$ and $_2(-1,0)_n^+$ resonances, calculated with a matching radius of $R = 6.5$ a.u., compared to the diabatic-by-sector results of Ref. [17].

Resonance	Present result (a.u.)	Reference [17] (a.u.)
$_2(+1,0)_2^+$	−0.7717	−0.7774
$_2(-1,0)_2^+$	−0.6170	−0.6218
$_2(+1,0)_3^+$	−0.5952	−0.5902
$_2(-1,0)_3^+$	−0.5493	−0.5479
$_2(+1,0)_4^+$	−0.5447	−0.5452
$_2(-1,0)_4^+$	−0.5280	−0.5277
$_2(+1,0)_5^+$	−0.5262	−0.5269

impractical for determining higher-lying resonances below the $N = 2$ threshold, because of the large number of harmonics required to follow the channels into their potential valleys. We therefore superpose instead accurate adiabatic channels [34] according to boundary conditions established by the R matrix evaluated at a matching radius R_0, transforming the core's information from an R matrix to a short-range reaction matrix K (Sec. 9.3 of [13]). We then apply boundary conditions as $R \to \infty$ to "eliminate" the closed channels according to standard multichannel quantum defect theory [12,13]. Table III shows the resulting resonance positions calculated with a matching radius of $R = 6.5$ a.u. near the apparent core radius in Fig. 5. The positions agree with the accurate calculations of Ref. [17] to within the same accuracy as the bound state results reported above. Similarly, the widths of the resonances compare with those of several alternative calculations, as shown in Table IV.

We conclude that *all* the autoionizing resonances of $^1S^e$ symmetry below the $N = 2$ threshold of helium decay primarily through their interactions with the open channel at $R \sim 3.5$ a.u. Put another way, the doubly excited electron pair withdraws to 3.5 a.u. where the electrons scatter, furnishing a single electron with sufficient energy to leave the atom. Resonances belonging to other symmetries need not decay by collapsing to small R; the ρ eigenchannels should nevertheless uncover their decay routes.

TABLE IV. Widths, in eV, of the resonances in Table III, compared to calculations based on diabatic-by-sector [17], close-coupling [35], and "saddle-point" [36] methods. The numbers in brackets denote the power of ten by which the width is multiplied.

Resonance	Present result (eV)	Reference [17] (eV)	Reference [35] (eV)	Reference [36] (eV)
$_2(+1,0)_2^+$	1.0[−1]	1.2[−1]	1.3[−1]	9.1[−2]
$_2(-1,0)_2^+$	9.0[−3]	4.9[−3]	6.3[−3]	1.8[−2]
$_2(+1,0)_3^+$	2.7[−2]	3.7[−2]	3.8[−2]	2.5[−2]
$_2(-1,0)_3^+$	5.4[−3]	9.2[−4]	2.3[−4]	6.9[−3]
$_2(+1,0)_4^+$	5.0[−3]	1.4[−2]	1.3[−2]	1.1[−2]
$_2(-1,0)_4^+$	2.4[−3]	4.0[−4]	1.4[−3]	2.6[−3]
$_2(+1,0)_5^+$	2.2[−3]	6.4[−3]	5.7[−3]	5.3[−3]

IV. CONCLUSIONS

This paper has shown how the hyperradial development of the total phase eigenchannels illuminates the structure of channel coupling, pointing to the dominant role of *phase degeneracies* localized in narrow regions of R. Preliminary investigation of higher-lying resonances has reproduced general conclusions already present in the adiabatic approach, namely, the approximate autoionization selection rules $N \to N - 1$, $K \to K - 1$ [19]. These approximate selection rules break down near the double-ionization threshold, where the level of the "Ns^2" state lies below the $(N - 1)$th single-ionization threshold into which it would otherwise decay [37]. The systematic study of the R-matrix eigenchannels at higher energies should reveal the excitation mechanisms and selection rules applicable in this regime where the adiabatic approximation is no longer valid; this study will appear in future work.

Still more importantly, we emphasize again the utility of hyperspherical coordinates for describing atomic and molecular systems with an arbitrary number of constituents [23,22]. The R-matrix eigenchannel method described in Sec. II thus affords an opportunity for a unified view of all configurations of chemical species and of their transitions. Preliminary applications to molecular hydrogen are currently underway [38].

[1] J. L. Bohn and U. Fano, Phys. Rev. A **50**, 2893 (1994).

[2] C. Zemach, Nuovo Cimento **33**, 939 (1964); A. Degasperis, *ibid.* **34**, 1667 (1964); F. Calogero, *Variable Phase Approach to Potential Scattering* (Academic, New York, 1967).

[3] U. Fano and E. Y. Sidky, Phys. Rev. A **45**, 4776 (1992); E. Y. Sidky, *ibid.* **47**, 2812 (1993).

[4] J. L. Bohn, Phys. Rev. A **49**, 3761 (1994).

[5] M. H. Alexander, J. Chem. Phys. **95**, 8931 (1991); D. E. Manolopoulos and M. H. Alexander, *ibid.* **97**, 2527 (1992).

[6] W. E. Milne, Phys. Rev. **35**, 863 (1930).

[7] E. Young, Phys. Rev. **38**, 1613; *ibid.* **39**, 455 (1932).

[8] F. Robicheaux, U. Fano, M. Cavagnero, and D. A. Harmin, Phys. Rev. A **35**, 3619 (1987).

[9] E. Y. Sidky (unpublished).

[10] P. F. O'Mahoney and C. H. Greene, Phys. Rev. A **31**, 250 (1985).

[11] P. G. Burke and K. A. Berrington, *Atomic and Molecular Processes – An R-Matrix Approach* (Institute of Physics Publishing, Bristol, 1993).

[12] M. J. Seaton, Rep. Prog. Phys. **46**, 167 (1983).

[13] U. Fano and A. R. P. Rau, *Atomic Collisions and Spectra* (Academic, Orlando, 1986).

[14] R. Bellman and G. M. Wing, *An Introduction to Invariant Imbedding* (Wiley-Interscience, New York, 1975); B. R. Johnson, J. Comput. Phys. **13**, 445 (1973).

[15] J. C. Light and R. B. Walker, J. Chem. Phys. **65**, 4272 (1976).

[16] B. I. Schneider and R. B. Walker, J. Chem. Phys. **70**, 2466 (1979); B. I. Schneider and H. S. Taylor, *ibid.* **77**, 379 (1982).

[17] J. Tang, S. Watanabe, and M. Matsuzawa, Phys. Rev. A **46**, 2437 (1992).

[18] J. Macek, J. Phys. B **1**, 831 (1968).

[19] C. D. Lin, Adv. At. Mol. Phys. **22**, 77 (1986).

[20] H. Fukuda, N. Koyama, and M. Matsuzawa, J. Phys. B **20**, 2959 (1987).

[21] Y. F. Smirnov and K. V. Shitikova, Fiz. Elem. Chastits. At. Yadra. **8**, 847 (1977) [Sov. J. Part. Nucl. **8**, 344 (1977)].

[22] U. Fano, Phys. Rev. A **24**, 2402 (1981).

[23] M. Cavagnero, Phys. Rev. A **30**, 1169 (1984); **33**, 2877 (1986); **36**, 523 (1987).

[24] R. D. Mattuck, *A Guide to Feynman Diagrams in the Many-Body Problem* (Dover, New York, 1992).

[25] M. Ya. Amusia, Adv. At. Mol. Phys. **17**, 1 (1981).

[26] V. A. Fock, Izv. Akad. Nauk. SSSR, Ser. Fiz. **18**, 161 (1954) [K. Nor. Vidensk. Selsk. Forh. **31**, 138 (1958); **31**, 145 (1958)]; see also T. H. Gronwall, Phys. Rev. **51**, 655 (1937); J. H. Bartlett, Jr., Phys. Rev. **51**, 661 (1937).

[27] C. H. Greene and J. L. Dehmer, Argonne National Laboratory Report No. ANL-77-65, Part I (unpublished); C. H. Greene, Phys. Rev. A **20**, 656 (1979).

[28] J. M. Feagin, J. Macek, and A. F. Starace, Phys. Rev. A **32**, 3219 (1985).

[29] C. D. Lin, Phys. Rev. A **10**, 1986 (1974).

[30] L. Zhang and A. R. P. Rau, Phys. Rev. A **46**, 6933 (1992).

[31] C. E. Moore, *Atomic Energy Levels* (National Bureau of Standards, Washington, 1949, 1971), p. 5.

[32] P. J. Hicks and J. Comer, J. Phys. B **8**, 1866 (1975).

[33] G. Wannier, Phys. Rev. **90**, 817 (1953); A. R. P. Rau, Phys. Rev. A **4**, 207 (1971); R. Peterkop, J. Phys. B **4**, 513 (1971); A. R. P. Rau, *ibid.* **16**, L699 (1983).

[34] H. R. Sadeghpour, Phys. Rev. A **43**, 5821 (1991); H. R. Sadeghpour, J. Phys. B **25**, L29 (1992).

[35] D. H. Oza, Phys. Rev. A **33**, 824 (1986).

[36] L. Wu and J. Xi, J. Phys. B **23**, 727 (1990).

[37] J. Müller, X. Yang, and J. Burgdörfer, Phys. Rev. A **49**, 2470 (1994).

[38] A. Lidz (unpublished).